Chapter 8

RELATIVISTIC HYDRODYNAMICS

Classical fluid dynamics is unable to capture interesting phenomena produced by the coupling of space and time in the framework of the special and general theory of relativity. In the last decade, high-resolution finite volume schemes based on the solution of Riemann problems have played an important role in the advancement of numerical solutions to the partial differential equations governing inviscid, non-heat conducting, relativistic fluid dynamics (e.g., see [6], [21], [22], [23], [38], [52], [54], [65], [67]). These schemes have been successfully applied in ultra-relativistic regimes where the relativistic effects are important because of the following:

1. The fluid pressure is comparable to the mass density, causing the internal fluid energy to become relativistic.

2. The fluid has a bulk velocity that approaches the speed of light.

3. The fluid dynamics occur in the vicinity of a compact object like a black hole or neutron star.

Old schemes based on artificial viscosity used by Wilson [82] and others [13], [31] were unable to cope with such ultra-relativistic flows. Most high energy astrophysical flows require a relativistic treatment, making applications of relativistic fluid dynamics numerous.

In previous chapters of this thesis we developed a new high-resolution wave propagation algorithm to solve conservation laws on manifolds. The new algorithm has been applied to various classical equations including the Euler equations, and the scalar field equation. In this chapter, applications for relativistic hydrodynamics are presented. The examples are chosen from the literature and represent a preliminary set of tests for the algorithm. Future work, as described in Chapter 9, will involve a more detailed analysis of the performance of the algorithm for relativistic systems.

8.1 Einstein's relativity theory

Albert Einstein introduced the special theory of relativity in 1905. This theory revolutionized the way in which scientists think about space and time. The understanding of time before relativity theory was clearly stated by Newton in the *Principia*, "Absolute, true, and mathematical time, of itself, and from its own nature, flows equably without relation to anything external". This Newtonian notion of absolute time is replaced with a notion of the relative passage of time. Two different observers in spacetime need not agree on the passage of time between the same events. Einstein based the special theory of relativity on two simple principles :

- *No experiment can measure the absolute speed of a spacetime observer.*

- *The speed of light is a universal constant.*

In this thesis we consider units in which the speed of light, c, has the value $c = 1$.

Special relativity is a great success in many areas of physics, however, it is inconsistent with a Newtonian theory of gravity in which the field propagates with infinite speed (*violating the second principle*). In 1915, Einstein made another fundamental contribution to science by introducing the general theory of relativity. The general theory postulates that gravitational forces are not forces in the Newtonian sense, but are generated by a geometric tidal field tensor related to the source density of gravitational field. The theory predicts that free particles travel on geodesics of the spacetime geometry. If there is a local concentration of energy, geodesics in this region will converge (*since the energy density of normal matter is positive*) and observers traveling past this region would precieve a force as the geodesic path deviates from a straight line. An important principal of the general theory insures local consistency with the special theory of relativity. This principle in called the strong equivalence principle and says the following :

- *In a neighborhood of each event in spacetime, physical laws take on their special relativistic form.*

The strong equivalence principle will enable us to solve general relativistic Riemann problems using locally special relativistic frames. This is essentially the same process used to solve Riemann problems in orthonormal frames as described in Chapter 6. The first application of this can be found in [67].

The equations governing the dynamics of the gravitational field in the presence of matter can be written in the simple and elegant form

$$\overset{\leftrightarrow}{G} = 8\pi\overset{\leftrightarrow}{T}. \tag{8.1}$$

The Einstein tensor, $\overset{\leftrightarrow}{G}$, is a second rank symmetric tensor in four dimensions (one time-like and three space-like) that contains information about the spacetime metric and its derivatives. The energy momentum tensor $\overset{\leftrightarrow}{T}$ is also of second rank and symmetric, but contains information about matter fields, e.g., electrodynamic or hydrodynamic. The Einstein equations (8.1) describe the way in which matter generates spacetime curvature, and in turn, the curvature of spacetime modifies the flow of matter.

It was mentioned in Chapter 1 that the simple appearance of equation (8.1) is quite deceiving, and simple solutions exist only when one considers systems with physically restrictive symmetries. In fact, the Einstein equations (8.1) are a system of ten nonlinear partial differential equations in one time-like variable, and three spatial variables. In order to solve these equations with little or no symmetry, one must turn to numerical approximations. The numerical evolution of the Einstein equations, however, is also a very difficult task. Shapiro and Teukolsky [72], [73] suggest four requirements for a successful numerical code in relativity. They claim the code should (1) avoid singularities, (2) handle black hole

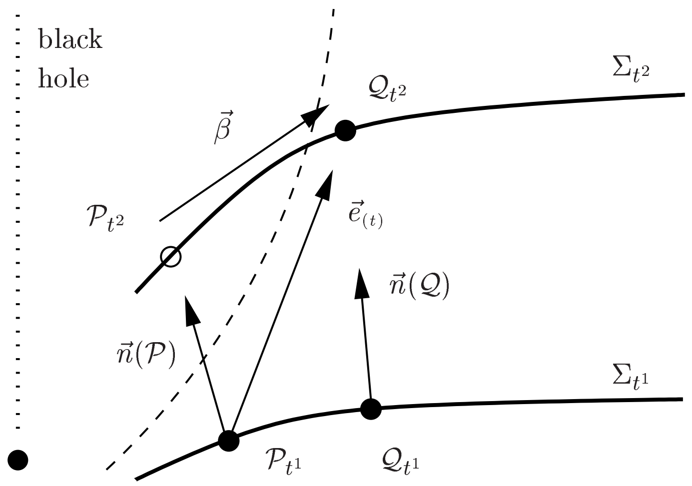

Figure 8.1: $\{3+1\}$ foliation of spacetime showing the role of the shift vector $\vec{\beta}$.

spacetimes, (3) maintain high accuracy, and finally, (4) run forever. These were suggested in 1986, yet there exists no code today (*to the author's knowledge*) that satisfies all of these requirements given moderately general initial and boundary conditions for the fields. For this reason, it is the opinion of the author that, at this time, it is important to develop accurate and stable algorithms not for the full problem, but for systems governed by the simplifications discussed in Chapter 1. Therefore, in the rest of this chapter we focus on the test fluid approximation in which the metric is not evolved in time. Applications of wave propagation algorithms in numerical relativity can be found in Bardeen and Buchman [7].

8.2 {3+1} Foliation of Spacetime

The numerical solution of equations (8.1) usually takes place in the framework of the $\{3+1\}$ formalism [2],[35], [36]. This formalism views the four dimensional spacetime $\{\mathscr{M}, \overleftrightarrow{g}\}$ as a time-foliation of three dimensional space-like hypersurfaces $\{\Sigma_t\}$. Such hypersurfaces are constructed by laying down a coordinate system and holding the time coordinate constant. Each Σ_t has a three-dimensional Riemannian metric $[h_{ij}]$, where here and in what follows Latin indices range over spatial coordinates (i.e. $i, j, k, etc. \in \{1,2,3\}$), and Greek indices range over spacetime (i.e. $\alpha, \beta, \mu, etc. \in \{0,1,2,3\}$).

We define *Eulerian* observers, ϑ_E, as those frames at rest in the spatial hypersurface Σ_{t^1}. These Eulerian observers have a four velocity equal to the time-like unit normal at each point of the hypersurface. Two such frames are shown in figure 8.1 at points $\mathcal{P}_{t^1}$ and $\mathcal{Q}_{t^1}$ with the associated time-like unit normals $\vec{n}(\mathcal{P})$ and $\vec{n}(\mathcal{Q})$, respectively. If the observer at $\mathcal{P}$ adopted the non-coordinate basis $\{\vec{n}, \vec{e}_{(j)}\}$, then the spacetime metric in that frame has the form

$$ds^2 = -d\tau^2 + h_{ij} dx^i \, dx^j, \tag{8.2}$$

$$[g_{\mu\nu}] = \begin{pmatrix} -1 & 0 \\ 0 & h_{ij} \end{pmatrix}, \tag{8.3}$$

$$[g^{\mu\nu}] = \begin{pmatrix} -1 & 0 \\ 0 & h^{ij} \end{pmatrix}, \tag{8.4}$$

where τ is the proper time for the Eulerian observer. Figure 8.1 shows an Eulerian observer leaving $\mathcal{P}_{t^1} \in \Sigma_{t^1}$, and arriving at $\mathcal{P}_{t^2} \in \Sigma_{t^2}$ after a time $\Delta\tau$. A *spacetime* observer, ϑ_S, with coordinates $x^\mu = \{t, x^i\}$ and basis $\{\vec{e}_{(t)}, \vec{e}_{(i)}\}$ would follow the same path to find an elapsed time $\Delta\, t = N(x^\mu)\, \Delta\, \tau$, and spatial coordinates $x^i(\mathcal{P}_{t^2}) = x^i(\mathcal{P}_{t^1}) - \vec{\beta}\, \Delta\, t$. In these coordinates, the spacetime metric has the form

$$ds^2 = -N^2 \, dt^2 + h_{ij}(dx^i + \beta^i \, dt)(dx^j + \beta^j \, dt), \tag{8.5}$$

$$[g_{\mu\nu}] = \begin{pmatrix} -N^2 + \beta_i \, \beta^i & \beta_j \\ \beta_i & h_{ij} \end{pmatrix}, \tag{8.6}$$

$$[g^{\mu\nu}] = \begin{pmatrix} -1/N^2 & \beta^j/N^2 \\ \beta^i/N^2 & h^{ij} - \beta^i \, \beta^j/N^2 \end{pmatrix}, \tag{8.7}$$

where the lapse function, $N(x^\mu)$, and a shift vector, $\vec{\beta}$ have been introduced. Using equations (8.6) and (8.7), it is easy to show that

$$\sqrt{-g} = N \sqrt{h}, \tag{8.8}$$

where we have used the notation $g = \det(\overleftrightarrow{g})$ and $h = \det(\overleftrightarrow{h})$. We will make extensive use of this fact in the development of relativistic hydrodynamics.

8.3 Relativistic Hydrodynamics

The flow of a relativistic gas is governed by the local conservation of both matter and energy-momentum

$$\check{\nabla} \cdot \check{J} = 0 \tag{8.9}$$

$$\check{\nabla} \cdot \overleftrightarrow{T} = 0, \tag{8.10}$$

where $\check{\nabla}$ is the spacetime covariant derivative, $\check{J}$ is the current of rest mass, and $\overleftrightarrow{T}$ is the stress-energy tensor from equation (8.1). In terms of the primitive variables of the flow these have the form

$$\check{J} = \rho \, \check{u} \tag{8.11}$$

$$\overleftrightarrow{T} = \rho \, \varepsilon \, \check{u} \otimes \check{u} + p \, \overleftrightarrow{g}, \tag{8.12}$$

where ρ is the proper gas density, $\breve{u}$ is the four velocity of the flow, and ε is the relativistic specific enthalpy

$$\varepsilon = 1 + \epsilon + p/\rho, \tag{8.13}$$

ϵ being the specific internal energy of the fluid. These equations are closed by the normalization of the four velocity, $\breve{u} \cdot \breve{u} = -1$, and an equation of state $p \to p(\rho, \epsilon)$. In the examples presented here we assume an equation of state for a perfect gas

$$p(\rho, \epsilon) = (\gamma - 1)\ \rho\, \epsilon, \tag{8.14}$$

where γ is a constant.

We write down the conservation laws (8.9) and (8.10) on a coordinate basis adopted by spacetime observers ϑ_S discussed in Section 8.2 with basis $\{\vec{e}_{(\alpha)}\}_{\vartheta_S} = \{\vec{\partial}_{(t)}, \vec{\partial}_{(i)}\}$. Flow quantities, however, are most naturally measured by Eulerian observers at rest in the hypersurface with basis $\{\vec{e}_{(\bar{\alpha})}\}_{\vartheta_E} = \{\hat{n}, \vec{\partial}_{(i)}\}$. These bases are related by $\vec{e}_{(\alpha)} = \Pi^{\bar{\beta}}_{\alpha}\, \vec{e}_{(\bar{\beta})}$, with

$$[\Pi^{\bar{\beta}}_{\alpha}] = \left(\begin{array}{cc} N & 0 \\ \beta^i & \mathcal{I}^{ij} \end{array} \right). \tag{8.15}$$

Using (5.16) and (5.17), it is easy to show that the components of four velocities transform between the two bases as

$$u^{\bar{0}} = N\, u^t \tag{8.16}$$

$$u^{\bar{i}} = u^i + u^t\, \beta^i, \tag{8.17}$$

and similarly

$$u_{\bar{0}} = u^t/N - \left(\beta^k\, u_k\right)/N \tag{8.18}$$

$$u_{\bar{i}} = u^i. \tag{8.19}$$

We can use these relationships to compute properties of the flow in the frame for which the calculation is simple. For example, observers ϑ_E experience a flow Lorentz factor

$$\begin{aligned} W &= -\hat{n} \cdot \breve{u} \\ &= u_{\bar{0}} \\ &= N\, u^t, \end{aligned} \tag{8.20}$$

where we have used the fact that $u_{\bar{0}} = u^{\bar{0}}$ in the frame of ϑ_E. It follows that observers ϑ_E measure a flow velocity of

$$v_i = \frac{\breve{u} \cdot \vec{e}_{(\bar{i})}}{W} \tag{8.21}$$

with contravariant components

$$v^i = u^i/W + \beta^i/N. \tag{8.22}$$

The normalization of the four velocity $\breve{u} \cdot \breve{u} = -1$ allows us to represent the Lorentz factor in the familiar way,

$$W = \frac{1}{\sqrt{1 - \vec{v} \cdot \vec{v}}}, \tag{8.23}$$

where $\vec{v} \cdot \vec{v} = h_{ij}\, v^i\, v^j$.

Consider the set of four vectors

$$\mathscr{Q} = \{\check{J}, \check{s}_{(i)}, \check{e}\}, \tag{8.24}$$

where, once again, $\check{J}$ is the rest-mass current density, $\check{s}_{(i)}$ is the momentum four vector in the $\vec{e}_{(i)}$ direction, and $\check{e}$ is the energy four vector defined as

$$\check{s}_{(i)} = \overleftrightarrow{T}(\vec{e}_{(i)}, \cdot) = \rho\, \varepsilon\, u_i\, \check{u} + p\, \overleftrightarrow{g}(\vec{e}_{(i)}, \cdot) \tag{8.25}$$

$$\check{e} = -\overleftrightarrow{T}(\hat{n}, \cdot) = \rho\, \varepsilon\, W\, \check{u} + p\, \overleftrightarrow{g}(\hat{n}, \cdot). \tag{8.26}$$

We can write the conservation laws (8.9) and (8.10) in terms of the set $\mathscr{Q}$ of four vectors

$$\check{\nabla} \cdot \mathscr{Q} = \mathscr{S}, \tag{8.27}$$

where, due to the chain rule, the source term has the form

$$\mathscr{S} = \{0, \overleftrightarrow{T} : \check{\nabla}\vec{e}_{(i)}, \overleftrightarrow{T} : \check{\nabla}\hat{n}\}. \tag{8.28}$$

Since we are writing the conservation laws onto the coordinate basis of ϑ_S, but we have covariant derivatives of the basis for ϑ_E, we will have the introduction of Christoffel symbols in the source term. We can write

$$\begin{aligned} \overleftrightarrow{T} : \vec{e}_{(i)} &= T^{\alpha\beta}\, \nabla_\alpha \vec{e}_{(i)\beta} \\ &= T^{\alpha\beta} \left(g_{i\beta,\alpha} - \Gamma^{\delta}_{\beta\alpha}\, g_{i\delta} \right). \end{aligned} \tag{8.29}$$

Similarly, for the energy equation we can write

$$\begin{aligned} \overleftrightarrow{T} : \hat{n} &= T^{\alpha\beta} \nabla_\alpha \hat{n}_\beta \\ &= N \left(T^{\alpha t} \left(\log N\right)_\alpha - T^{\alpha\beta}\, \Gamma^{t}_{\beta\alpha} \right). \end{aligned} \tag{8.30}$$

We now define our state variables in terms of the time components of the four vectors above

$$\boldsymbol{q} = \begin{pmatrix} -\check{J}(\hat{n}) \\ -\check{s}_{(i)}(\hat{n}) \\ -\check{e}(\hat{n}) \end{pmatrix} \equiv \begin{pmatrix} D \\ S_i \\ E \end{pmatrix}. \tag{8.31}$$

The conservation laws can now be written in standard form

$$\frac{\partial}{\partial t}\boldsymbol{q} + \frac{1}{\sqrt{h}} \left(N \sqrt{h}\, \boldsymbol{f}^{(k)} \right)_{,k} = N \boldsymbol{\psi}, \tag{8.32}$$

where we have made use of the fact that, for a four-vector $\check{X}$, $-\check{X}(\hat{n}) = N\, X^t$, so that, for example, $D = N\, J^t$ and the fluxes have the form

$$\boldsymbol{f}^{(k)} = \begin{pmatrix} D \left(v^k - \beta^k/N\right) \\ S_j \left(v^k - \beta^k/N\right) + p \delta^k_j \\ E \left(v^k - \beta^k/N\right) + p\, v^k \end{pmatrix}. \tag{8.33}$$

8.3.1 Computational difficulties

Though equations (8.50) with flux (8.33) look similar to the classical Euler equations, there are differences that pose computational difficulties worth mentioning. These difficulties can be summarized as follows:

1. One consequence of relativity theory is that mass and energy are proportional (*Einstein's famous* $E = mc^2$). The constant of proportionality $c^2 \sim 10^{17} m^2/s^2$ is very large and so the energy density $E = T^{tt}$ is dominated by the rest mass contribution. Capturing dynamics of the fluid's thermodynamic energy is difficult because of the relative size of the mass contribution. Numerically it makes sense to define an energy perturbation denoted here by $\tau = E - D$, where we note that we are working in units with $c = 1$. Subtracting D from E effectively removes the rest mass energy as measured by observers ϑ_S. It is τ that is used in the conserved vector $\boldsymbol{q}$
$$\boldsymbol{q} = \begin{pmatrix} -\check{J}(\hat{n}) \\ -\check{s}_{(i)}(\hat{n}) \\ -\check{e}(\hat{n}) + \check{J}(\hat{n}) \end{pmatrix} \equiv \begin{pmatrix} D \\ S_i \\ \tau \end{pmatrix}, \tag{8.34}$$
with the following modifications to the flux:
$$\boldsymbol{f}^{(k)} = \begin{pmatrix} D\left(v^k - \beta^k/N\right) \\ S_j\left(v^k - \beta^k/N\right) + p\delta_j^k \\ \tau\left(v^k - \beta^k/N\right) + p\, v^k \end{pmatrix}. \tag{8.35}$$

2. The solution of Riemann problems in most hydrodynamic codes involves using primitive variables of the system, for example, $\{\rho, u_i, p\}$, the density, components of velocity, and pressure, respectively. The algebraic relationship between primitive and conserved variables must be inverted at each time step. This algebraic relationship for a classical inviscid perfect gas has the form
$$\begin{aligned} \rho &= \rho \\ s_i &= \rho\, u_i \\ E &= \frac{p}{\gamma - 1} + \frac{1}{2}\rho \vec{u}\cdot\vec{u}, \end{aligned} \tag{8.36}$$
which is trivially inverted. However, this is not the case for the equations of relativistic hydrodynamics. The relationship between the conserved and primitive variables for this system is
$$\begin{aligned} D &= \rho\, W, \\ S_i &= \rho\, \varepsilon\, W^2\, v_i, \\ \tau &= \rho\, \varepsilon\, W^2 - p - \rho\, W. \end{aligned} \tag{8.37}$$
The difficulty arises due to the presence of the Lorentz factor $W = (1 - \vec{v}\cdot\vec{v})^{-1/2}$, which nonlinearly couples the sets of variables in relativistic regimes for which $W > 1$. An iterative procedure is needed to carry the inversion out in each time step. We follow the procedure discussed in [56] for an equation of state for a perfect gas, $p = (\gamma - 1)\epsilon\rho$.

(a) Define a function

$$f(\tilde{p}) = \tilde{p} - (\gamma - 1)\, \epsilon_\star(\tilde{p})\, \rho_\star(\tilde{p}). \tag{8.38}$$

(b) Compute a $W_\star$ based on the velocity

$$v_i = \frac{S_i}{p + D + \tau}. \tag{8.39}$$

(c) Use $W_\star$ to compute

$$\rho_\star = \frac{D}{W_\star} \tag{8.40}$$

$$\epsilon_\star = \frac{\tau + D(1 - W_\star) + \tilde{p}(1 - W_\star^2)}{D\, W_\star}, \tag{8.41}$$

which gives a value of f to test for convergence.

The procedure is carried out using a bisection method as a predictor, and then a Newton iteration for accuracy.

3. Yet another complication arises in multidimensional relativistic hydrodynamics. Multidimensional finite volume Godunov-type algorithms rely on the solution of one-dimensional Riemann problems normal to each grid interface. The classical Euler equations fit very nicely into this framework due to the fact that the Riemann solution is completely determined by the density, pressure, and normal velocity. The transverse velocity is constant through all normal shock and rarefaction waves. It is the shear waves that carry the jumps in transverse velocities.

   Equations (8.50), however, do not retain this property. The coupling between the normal and transverse directions is expected due to the presence of W. It is not true that transverse velocities are constant through the shock and rarefaction waves of the one-dimensional Riemann problems. Balsara presents details as to how one handles this in [5]. In his paper, a 2-shock approximate Riemann solver treats the transverse velocity exactly for shock waves. In practice, one finds good results by ignoring this coupling. This is most likely due to the cell averaging procedure used in the solution of Riemann problems.

8.3.2 Special relativistic test fluids

The simplest relativistic test fluid is one that flows in Minkowski spacetime $(\mathscr{M}, \overleftrightarrow{\eta})$, where $\overleftrightarrow{\eta}$ is a stationary metric defined by

$$[\eta_{\alpha\beta}] = \mathrm{diag}(-1, 1, 1, 1), \tag{8.42}$$

in three spatial dimensions. The Minkowski metric is the relativistic analog of the Cartesian metric. Points in Minkowski spacetime are called events, and are denoted by the vector $\check{x} = (t, x^1, x^2, x^3)^T$ in three spatial dimensions.

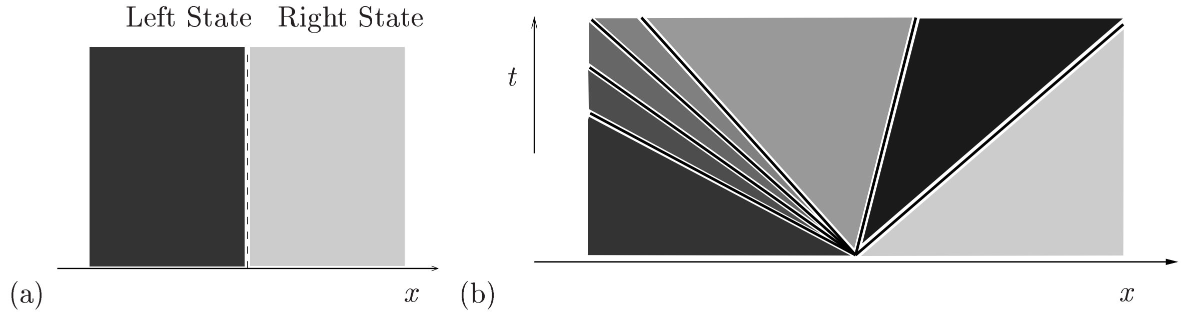

Figure 8.2: (a) Piecewise constant initial data with a jump across an interface. (b) Time evolution of the decay of this initial data.

A fluid element has four-velocity $\check{u} \equiv (d/d\tau)\check{x} = W(1, v^1, v^2, v^3)^T$, where τ is the proper time and $\vec{v}$ is the element's three-velocity. As previously discussed, the governing equations are the laws of local conservation of mass, momentum, and energy density. The energy momentum tensor $\overleftrightarrow{T}$, and the rest mass current density $\check{J}$ have components

$$\begin{aligned} T^{\alpha\beta} &= \rho h \, u^\alpha \, u^\beta + p \, \eta^{\alpha\beta}, \\ J^\alpha &= \rho \, u^\alpha, \end{aligned} \tag{8.43}$$

where ρ is rest mass density, $h = c^2 + \epsilon + p/\rho$ the relativistic specific enthalpy, ϵ the specific internal energy, and p is the fluid pressure. In an inertial (lab) frame with basis $\{\vec{\partial}_{(t)}, \vec{\partial}_{(i)}\}$, so that $[\nabla_\nu] = (\partial_t, \partial_{x^1}, \partial_{x^2}, \partial_{x^3})$, the conservation equations (8.50) can be written

$$\begin{aligned} & D_{,t} + \left(D \, v^k \right)_{,k} = 0 \\ & S^i{}_{,t} + \left(S^i \, v^k + p \, \delta^{ik} \right)_{,k} = 0 \\ & \tau_{,t} + \left(S^k - D \, v^k \right)_{,k} = 0, \end{aligned} \tag{8.44}$$

where i ranges over the spatial dimensions $\{1, \cdots, n_d\}$ and the definitions (8.37) have been used. An equation of state for a perfect gas

$$p = (\gamma - 1) \; \rho \, \epsilon, \tag{8.45}$$

closes equations (8.44), where γ is the ratio of specific heats for the fluid.

There are a number of well tested one dimensional examples in the literature. We present two such examples here, both will be Riemann problems with piecewise constant initial data. The initial setup is shown in Figure 8.2(a), and consists of two piecewise constant fluid states on each side of an imaginary membrane. The membrane is removed at $t = 0$, and the initial data decays into waves that propagate away from the interface as shown in Figure 8.2(b).

The first test problem consists of a high-pressure, dense gas on the left that expands into a less dense gas at low pressure. As this Riemann data decays, a left-going transonic

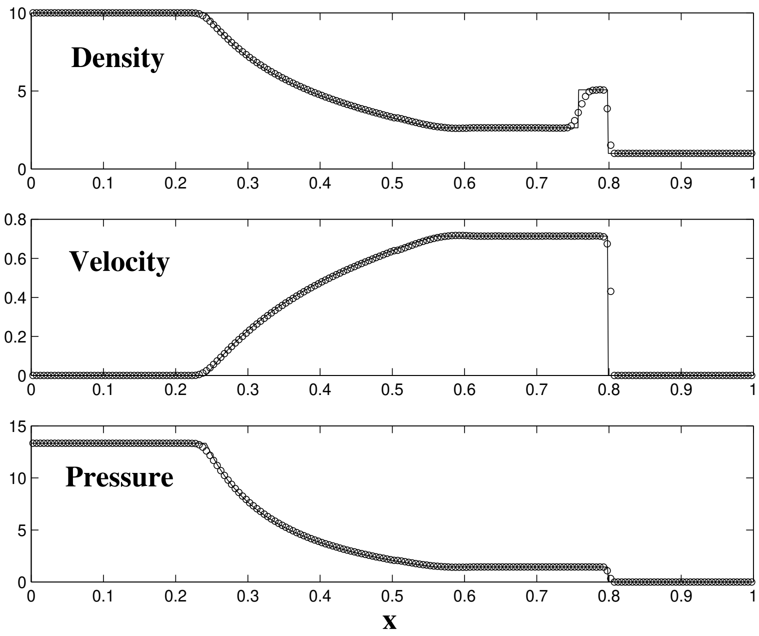

Figure 8.3: Comparison of computed solution and an exact solution for the first special relativistic example. The computed solution is shown as circles and the exact solution as a solid line.

rarefaction wave is produced. Numerically, the left variables at $t = 0$ are initialized to $\boldsymbol{q}_l = (\rho, u^x, p)^T = (10.0, 0.0., 13.3)^T$ and the right to $\boldsymbol{q}_r = (1.0, 0.0, 0.00000067)^T$. These numbers have been used in the literature, e.g., [55] and [57].

Figure 8.3 compares the solution generated by the wave propagation algorithm developed in this dissertation with an exact solution. In this figure, circles represent the computed solution and the solid line represents the exact solution. There are 100 cells across the domain in the computation and the gas constant was set to $\gamma = 5/3$. The new method compares well with those found in the literature, e.g., see [55] and [57]. The strong transonic rarefaction wave has been captured accurately, and the shock wave in the velocity is captured within two grid cells.

The second special relativistic Riemann problem presented in this section, also found in [55] and [57], involves a large jump in the pressure across the membrane. Once the initial data decays, the solution contains a thin dense shell created by a strong right-going shock. The left state at $t = 0$ is defined by $\boldsymbol{q}_l = (1.0, 0.0, 1000.0)^T$, and the right state by $\boldsymbol{q}_r = (1.0, 0.0, 0.01)^T$. This problem is more severe than the first example due to the fact that the pressure jumps by five orders of magnitude across the interface in the initial conditions.

Figure 8.4 shows the comparison of the computed solution with an exact solution. Once again, circles represent the computed solution and the solid line represents the exact solution.

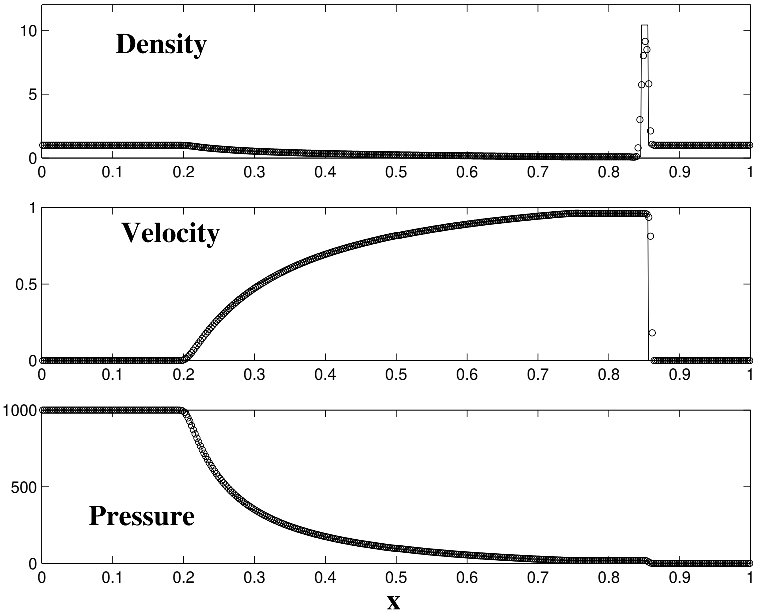

Figure 8.4: Comparison of computed solution and an exact solution for the second special relativistic example. The computed solution is shown as circles and the exact solution as a solid line.

The computations shown in this figure have been done with 400 cells across the domain. Once again, the gas constant was taken to be $\gamma = 5/3$. Notice that, once again, the strong shock in the velocity has been captured in two grid cells, and the rarefaction wave is accurately represented by the numerical results. The thin dense shell is also captured by the method.

8.3.3 Spherical accretion of dust onto a Schwarzschild black hole

In the next example, the relativistic accretion of dust onto a spherically symmetric black hole is computed. This test for the algorithm has been used by other authors, e.g., [6] and [31]. The assumption for this calculation is that the pressure remains negligible as the fluid particles flow inward along geodesics of the spacetime manifold. The geometry of the manifold is described by a metric that represents the Schwarzschild solution to the Einstein equations (8.1) with $\overset{\leftrightarrow}{T} = 0$. Using spherical coordinates, $\{t, r, \theta, \phi\}$, the Schwarzschild metric has the form

$$[g_{\alpha\beta}] = \begin{pmatrix} 1 - 2M/r & 0 & 0 & 0 \\ 0 & \frac{1}{1-2M/r} & 0 & 0 \\ 0 & 0 & r^2 & 0 \\ 0 & 0 & 0 & r^2 \sin^2(\theta) \end{pmatrix}, \tag{8.46}$$

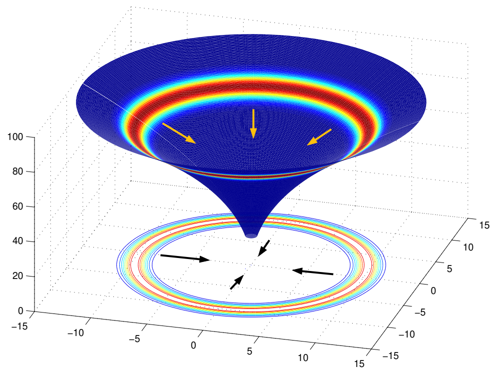

(a) Schwarzschild Black Hole

Figure 8.5: An embedding diagram of the Schwarzschild spacetime manifold with ϕ held fixed, and r and θ allowed to vary. Also depicted is a wave traveling towards the black hole singularity.

where M is the mass of the black hole. Notice that there is a singularity in the metric at $r = 2M$, the Schwarzschild radius. The metric singularity at this radius is only due to the coordinates, and can be removed by transforming to a new coordinate system. The only true spacetime singularity, e.g., where the curvature grows without bound, occurs at the center of the black hole.

Figure 8.5 shows an embedding diagram for a Schwarzschild black hole. The two-dimensional surface represents a function of the spacetime curvature along a slice with ϕ held fixed. Therefore, the surface is plotted in the coordinates $\{r, \theta\}$. This two-dimensional coordinate plane is discretized into the numerical domain $\{r_i, \theta_j\}$ with $r \in [r_0, r_f]$ and $\theta \in [\theta_0, \theta_f]$.

The initial conditions are those of vacuum, e.g., all variables are set to negligible values in each grid cell. The boundary conditions in the radial direction are set so that at $r = r_0$, zero-order outflow conditions are imposed, and at $r = r_f$ the exact inflow solution is imposed. In the θ-direction, there is no need to compute on the entire domain that has $\theta_f = 2\pi$. Instead, the computational domain is defined such that $\theta_f = \pi$, and symmetry preserving reflecting boundary conditions are used at both $\theta_0 = 0$ and $\theta_f = \pi$.

The initial data is allowed to evolve to a steady state, at which time the computed solution is compared with an exact solution. Figures 8.6(a) and 8.6(b) show the comparison of a computed solution with the exact solution on a grid with 160×60 cells after 2369 time steps. The solid lines represent the exact solution, while the circles represent computed values at all locations in the grid as a function of r. In the calculation shown, $r_0 = 2.2M$ and $r_f = 18M$.

The computed steady state compares well with the exact solution. However, notice that there is a small scatter in the data as r approaches $2M$. This is due to the fact

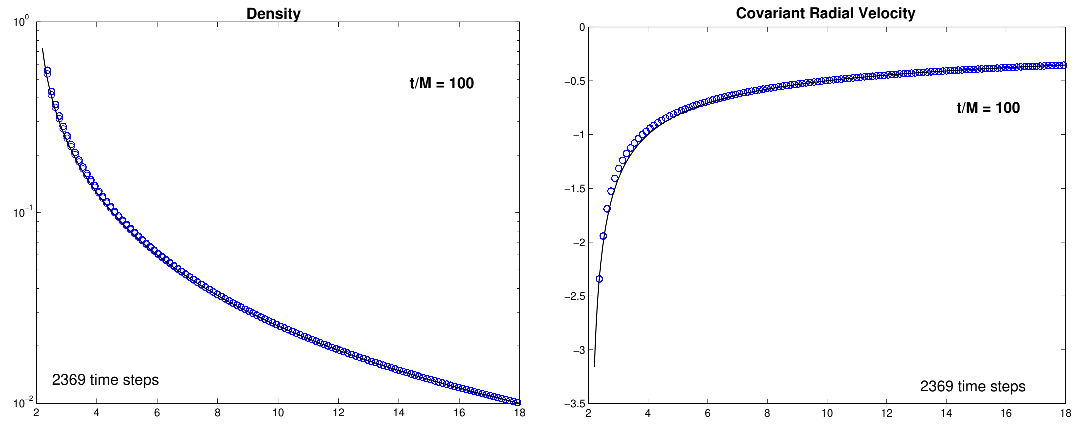

(a) Density

(b) Velocity

Figure 8.6: Spherically symmetric accretion of dust onto a Schwarzschild black hole. An exact solution is compared to the two-dimensional computed data as a function of r. The solid line represents the exact solution, and circles represent the computed data. (a) The steady state density profile. (b) The steady state radial coordinate velocity.

that the metric is singular near three of the four boundaries of the numerical domain. We have already discussed the singularity at the inner boundary where r is approaching the Schwarzschild radius. In addition to this, the metric (8.46) is also singular at both $\theta = 0$ and $\theta = \pi$.

This application is a good test of the algorithm for the following reasons first noted by Hawley, Smarr, and Wilson [31]:

- The problem tests the radial transport terms in the code. These terms show up in the spatially-varying flux functions since

  $$\det(\overset{\leftrightarrow}{h}) = \frac{r^4 \sin^2(\theta)}{1 - 2M/r}.$$

  It is the f-waves that handle these terms in the new algorithm.

- The problem also tests the ability of the method to handle general relativistic red-shift, and the effects of the lapse N.

- Finally, the problem tests that the code properly normalizes the four velocity of the fluid as needed in (8.23).

However, since the flow is only radial, the multidimensional components of the algorithm are not tested. For this, we turn to the next example.

8.3.4 Relativistic flow of an irrotational, isentropic perfect fluid

The relativistic Euler equations for an irrotational, isentropic perfect fluid have been formulated as a potential problem in several papers [24], [66]. This is done by making two assumptions:

1. The fluid obeys the equation of state $p = \rho \propto n^2$, where p is the pressure, ρ is the mass-energy density, and n is the baryonic number density.

2. The fluid is a perfect fluid with no vorticity.

Since the fluid has no vorticity, the velocity can be written as the gradient of a potential function

$$h\, u_\alpha = \varphi_{,\alpha}, \tag{8.47}$$

where $h = (p + \rho)/n$ is the specific enthalpy, and $\breve{u}$ is the four velocity of the fluid. The equation of continuity, together with assumption (2) above leads to an equation for φ that has the form

$$(\varphi^{,\alpha})_{;\alpha} = 0, \tag{8.48}$$

where, once again, the semi-colon represents the covariant derivative with respect to the spacetime metric, and a sum is implied on α. This equation is the relativistic extension of the scalar field equation studied in Chapter 6.

In this example, equation (8.48) is solved in a Schwarzschild spacetime generated by a massive hard sphere. The metric that describes the geometry is once again the Schwarzschild metric (8.46). The grid on which the calculation was done is the same grid that was used in the preceding example. Since ϕ is fixed, no derivatives with respect to that variable must be considered.

As we did for the scalar field equation of Chapter 6, we write equation (8.48) as a system of first-order conservation laws by defining the auxiliary variables:

$$p = \varphi_{,t}, \qquad \psi_r = \varphi_{,r}, \qquad \psi_\theta = \varphi_{,\theta}. \tag{8.49}$$

Using these variables in equation (8.48), the system that needs to be solved can be written as

$$\boldsymbol{q}_{,t} + \boldsymbol{f}^{(r)}_{,r} + \boldsymbol{f}^{(\theta)}_{,\theta} = \boldsymbol{\psi}, \tag{8.50}$$

where

$$\boldsymbol{q} = \left(p, \psi^r, \psi^\theta\right)^T \tag{8.51}$$

is the state vector of unknowns, and

$$\boldsymbol{f}^{(r)} = \left(-(1 - 2M/r)^2\, \psi^r, -p, 0\right)^T \tag{8.52}$$

is the flux along $\vec{\partial}_{(r)}$, and

$$\boldsymbol{f}^{(\theta)} = \left(1 - (1 - 2M/r)\, \frac{1}{r^2}\, \psi^\theta, 0, -p\right)^T \tag{8.53}$$

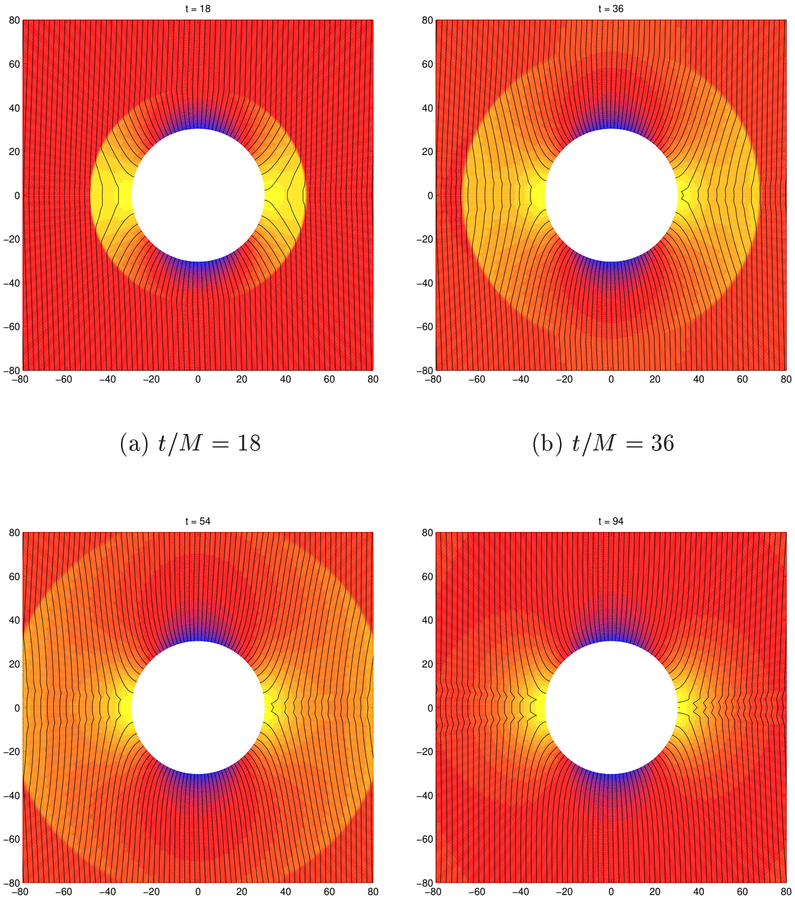

(a) $t/M = 18$ (b) $t/M = 36$

(c) $t/M = 54$ (d) $t/M = 94$

Figure 8.7: The time evolution of flow past a relativistic hard sphere. Plotted are the equi-potential lines of the flow. Particles travel along lines that are perpendicular to these contours.

is the flux along $\vec{\partial}_{(\theta)}$. Finally, the source terms that appear on the right hand side of equation (8.50) have the form

$$\boldsymbol{\psi} = \left((1 - 2M/r)\ (1 - 3M/r)\ \frac{2}{r}\,\psi^r + (1 - 2M/r)\,\frac{\cos(\theta)}{r^2\,\sin(\theta)}\,\psi^\theta, 0, 0 \right)^T . \tag{8.54}$$

Figures (8.7(a))-(8.7(d)) show the time evolution of a flow past the hard sphere. These figures show contours of equi-potential lines. Particles flow along paths that are perpendicular to these contours. The grid, $\{r_i, \theta_j\}$, in this calculation covers $r \in [30.4M, 700M]$ and $\theta \in [0, \pi]$ with 200 radial cells, and 60 cells in the θ-direction. The initial data has been set so that the flow is from left to right with

$$p(t=0) = -\left((1-2M/r)\left(1+(1-2M/r)\,\psi_{,r}^2 + \frac{1}{r^2}\psi_{,\theta}^2\right)\right)^{1/2} \tag{8.55}$$

$$\psi_r(t=0) = u_\infty \cos(\theta) \tag{8.56}$$

$$\psi_\theta(t=0) = -u_\infty\, r\, \sin(\theta), \tag{8.57}$$

where u_∞ is the right-going velocity at a large distance away from the sphere. The boundary conditions are such that at the outer radius of the grid, the conditions at infinity are imposed. At the surface of the sphere, the radial component of the velocity is reflected to ensure the behavior of a hard surface.

Notice that in Figures (8.7(a))-(8.7(d)) there is a sharp wave traveling outward from the surface of the sphere at the speed of light. The theory of relativity does not allow anything to travel faster than this wave. This wave represents the flow adjusting to the presence of the hard sphere. The out-going wave leaves behind it a steady-state flow around the hard sphere.